A Numerical Study of Flow and Pollutant Dispersion Characteristics in Urban Street Canyons

JONG-JIN BAIK AND JAE-JIN KIM

Department of Environmental Science and Engineering, Kwangju Institute of Science and Technology, Kwangju, Korea

(Manuscript received 29 May 1998, in final form 20 October 1998)

ABSTRACT

The flow and pollutant dispersion in urban street canyons are investigated using a two-dimensional numerical model with the k–ε turbulent closure scheme. It is shown that the flow field is characterized mainly by the number and intensity of vortices produced in the street canyon. As the street aspect ratio (ratio of the building height to the width between buildings) increases, the number of vortices increases. In the upper-canyon region, the downward motion near the downwind building is stronger than the upward motion near the upwind building, and the turbulent kinetic energy (TKE) is higher near the downwind building than near the upwind building because of stronger wind shears near the downwind building. The TKE budget analysis shows that the shear production is high near the interface between the ambient flow and the street canyon flow and that the turbulent dissipation is also high where the shear production is high. The horizontal advection and diffusion are found to play a crucial role in splitting the vortex into two or more. There is a critical value of the ambient wind speed above which the number and distribution pattern of vortices remain the same regardless of the ambient wind speed. For the given flow fields, two different emission sources (street-level source and advected source) are considered to examine pollutant dispersion in the street canyons that have a one-vortex flow regime and a two-vortex flow regime. Results indicate that the distribution of pollutant concentration in the street canyons during each period of continuous emission and nonemission can be largely explained in terms of the vortex circulation.

1. Introduction

An urban street canyon is the space between buildings that line up continuously along both sides of a relatively narrow urban street. With increasing urban population and industrial activities, the urban street canyon has resulted in a serious pollution problem. The hazardous materials from motor vehicles, heating and cooling systems of buildings, sudden fires, etc., can sicken or even cause fatal harm to humans within a polluted area. In order to minimize such casualties, it is necessary to understand and predict pollutant dispersion in street canyons. Studies of street canyons have been carried out as a basic research to understand flow and pollutant dispersion characteristics. Additionally, these basic studies have provided some guidelines of determining street dimensions for urban designers, who should take account of shelter effect, pollutant dispersion, urban warmth, solar access, and so on (Oke 1988).

Corresponding author address: Professor Jong-Jin Baik, Department of Environmental Science and Engineering, Kwangju Institute of Science and Technology, 572 Sangamdong, Kwangsan-ku, Kwangju 506-712, Korea.
E-mail: jjbaik@aromi.kjist.ac.kr

The climate of urban street canyons is mainly controlled by canyon geometry and meteorological conditions. An important parameter that has been widely used to represent canyon geometry is a street aspect ratio—a ratio of the building height to the width between buildings. Much attention has been paid to characterizing flow and dispersion in street canyons with different aspect ratios (e.g., Lee and Park 1994; Sini et al. 1996).

The flow regimes in urban street canyons can be categorized into the isolated roughness flow, the wake interference flow, and the skimming flow. These flow regimes are determined by the degree of the interaction between the vortex generated behind the upwind building and the downwind building (Hussain and Lee 1980; Oke 1988; Hunter et al. 1992; Sini et al. 1996). In three dimensions, the height-to-length ratio and the height-to-width ratio in a canyon are crucial factors determining flow regime. In two dimensions, the height-to-width ratio is a crucial factor determining flow regime. The inherent features in the three flow regimes are schematically drawn in Fig. 1. If the buildings are well apart, a low pressure recirculation vortex behind the upwind building due to the flow separation at the building top edge and a bolster eddy vortex due to the flow separation on the downwind wall (Sini et al. 1996) are formed. In

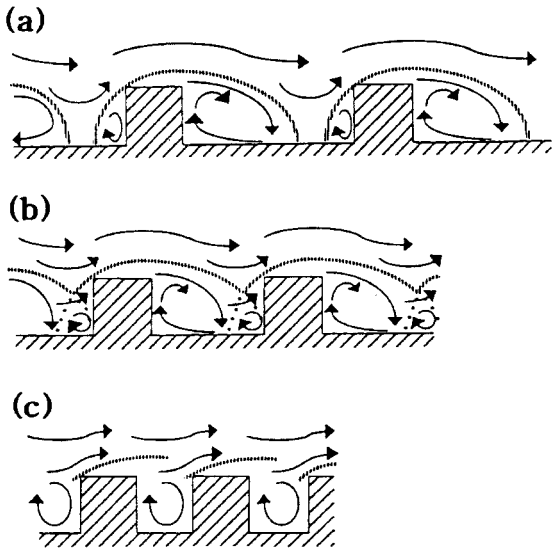

FIG. 1. Three flow regimes in urban street canyons: (a) isolated roughness flow, (b) wake interference flow, and (c) skimming flow [from Oke (1988)].

an isolated roughness flow, the flow recovers its upwind profile before the downwind building is encountered and the interaction between these two vortices (two corotating vortices) is negligible (Fig. 1a). If the buildings are less distant, the downwind building disturbs the recirculation vortex before readjustment can take place and interaction between the two vortices is possible, producing a wake interference flow (Fig. 1b). If the street canyon becomes narrow, the bulk of the above-roof flow does not enter the canyon and a stable vortex is established in the canyon, producing a skimming flow (Fig. 1c).

Studies of the isolated roughness flow (Nigim 1996; Hussein and Martinuzzi 1996; Zhang et al. 1996) have focused on the stagnation point at which flow diverges in front of the upwind building when the shear of the approaching flow exists, the reattachment point from which flow is readjusted to recover behind the vortex, the horseshoe vortex that results from the downward flow under the stagnation point and wraps around the upwind building, and the double-eddy circulation located on both corners behind the upwind building. Especially, the last two phenomena, which can also appear in the skimming flow and wake interference flow, are observed only in three dimensions and play an important role in distributing pollutant around the building. Hoydysh and Dabberdt (1988) showed that advection from the building corners to midblock by the double-eddy circulation presumably induces the convergence of pollutants and results in high-pollutant concentration at midblock.

In this study, we are concerned with the skimming flow regime. When the street aspect ratio is larger than a certain critical value, the counterrotating vortices located in the upper and lower regions of the street canyon emerge. The split of flow into two or three vortices stirs curiosity about their origin. An observational study in a street canyon of Chicago by DePaul and Sheih (1986) showed that an ambient wind speed of over 2 m s^{-1} is needed to maintain a single vortex in a street canyon with an aspect ratio of about 1.5. Using a numerical model, Lee and Park (1994) examined dispersion characteristics according to the flow condition and street aspect ratio. They showed that the removal of pollutants is effective for a shallow street canyon, while for a deep street canyon where two vortices develop, the pollutant transport from the lower vortex to the upper vortex is largely controlled by the diffusion process. Lanzani and Tamponi (1995) studied the influence of turbulence on the pollutant distribution using a Lagrangian particle model for nonhomogeneous turbulence and applied their new model to a generic urban topography.

In this study, we further investigate 1) how flow fields in urban street canyons are characterized with different street aspect ratios and ambient wind speeds and 2) how flow fields affect pollutant dispersion in the cases of street-level and advected pollutant sources. For this, we employ a two-dimensional numerical model with the k–ε turbulent closure scheme.

2. Description of numerical model

The numerical model used in this study is the same as that of Lee and Park (1994) except that the k–ε turbulent closure scheme is implemented for this study. We consider a two-dimensional, nonhydrostatic, nonrotating, incompressible airflow system without thermal effect and in momentum equations neglect molecular diffusion in comparison with turbulent diffusion. The momentum equations in the horizontal and vertical directions, the mass continuity equation, and the transport equation for pollutant concentration can be written as

$$\frac{\partial U}{\partial t} + U\frac{\partial U}{\partial x} + W\frac{\partial U}{\partial z} = -\frac{1}{\rho}\frac{\partial P}{\partial x} + \frac{\partial}{\partial x}\left(K_m\frac{\partial U}{\partial x}\right) + \frac{\partial}{\partial z}\left(K_m\frac{\partial U}{\partial z}\right), \quad (1)$$

$$\frac{\partial W}{\partial t} + U\frac{\partial W}{\partial x} + W\frac{\partial W}{\partial z} = -\frac{1}{\rho}\frac{\partial P}{\partial z} + \frac{\partial}{\partial x}\left(K_m\frac{\partial W}{\partial x}\right) + \frac{\partial}{\partial z}\left(K_m\frac{\partial W}{\partial z}\right), \quad (2)$$

$$\frac{\partial U}{\partial x} + \frac{\partial W}{\partial z} = 0, \quad (3)$$

and

$$\frac{\partial C}{\partial t} + U\frac{\partial C}{\partial x} + W\frac{\partial C}{\partial z} = \frac{\partial}{\partial x}\left(K_c\frac{\partial C}{\partial x}\right) + \frac{\partial}{\partial z}\left(K_c\frac{\partial C}{\partial z}\right) + S. \quad (4)$$

Here, ρ is the air density, U the mean velocity in the x direction, W the mean velocity in the z direction, P the mean pressure deviation, and C the mean concentration of a passive pollutant. The turbulent diffusivities for momentum and scalar variables are, respectively, K_m and K_c, and S in (4) denotes the source or sink term of pollutants.

To determine the turbulent diffusivities, the equations of turbulent kinetic energy (k) and its dissipation (ε) are included in the model (k–ε scheme). These are given in the present flow system by

$$\frac{\partial k}{\partial t} + U\frac{\partial k}{\partial x} + W\frac{\partial k}{\partial z} = K_m\left\{2\left[\left(\frac{\partial U}{\partial x}\right)^2 + \left(\frac{\partial W}{\partial z}\right)^2\right] + \left(\frac{\partial U}{\partial z} + \frac{\partial W}{\partial x}\right)^2\right\} + \frac{\partial}{\partial x}\left(\frac{K_m}{\sigma_k}\frac{\partial k}{\partial x}\right) + \frac{\partial}{\partial z}\left(\frac{K_m}{\sigma_k}\frac{\partial k}{\partial z}\right) - \varepsilon, \quad (5)$$

$$\frac{\partial \varepsilon}{\partial t} + U\frac{\partial \varepsilon}{\partial x} + W\frac{\partial \varepsilon}{\partial z} = C_{\varepsilon 1}\frac{\varepsilon}{k}K_m\left\{2\left[\left(\frac{\partial U}{\partial x}\right)^2 + \left(\frac{\partial W}{\partial z}\right)^2\right] + \left(\frac{\partial U}{\partial z} + \frac{\partial W}{\partial x}\right)^2\right\} + \frac{\partial}{\partial x}\left(\frac{K_m}{\sigma_\varepsilon}\frac{\partial \varepsilon}{\partial x}\right) + \frac{\partial}{\partial z}\left(\frac{K_m}{\sigma_\varepsilon}\frac{\partial \varepsilon}{\partial z}\right) - C_{\varepsilon 2}\frac{\varepsilon^2}{k}, \quad (6)$$

where

$$K_m = C_\mu\frac{k^2}{\varepsilon}, \quad (7)$$

$$\mathrm{Sc}_t = \frac{K_m}{K_c}. \quad (8)$$

The terms on the right-hand side of (5) and (6) represent the shear production term, turbulent diffusion terms in the x and z directions, and dissipation term, respectively. In (8), Sc is the turbulent Schmidt number. Following Sini et al. (1996), constants in (5)–(8) are specified as follows:

$$(C_\mu, \sigma_k, \sigma_\varepsilon, C_{\varepsilon 1}, C_{\varepsilon 2}, \mathrm{Sc}_t) = (0.09, 1.0, 1.3, 1.44, 1.92, 0.9). \quad (9)$$

The above governing equations are solved numerically on a staggered grid system using the finite volume method (finite area in two dimensions) following the solution algorithm described by Patankar (1980). In this algorithm, at each time step the tentative horizontal and vertical velocities are first obtained under an assumed pressure field. Then, the pressure change needed to adjust the velocity field so as to satisfy the mass continuity is calculated by solving a pressure-Poisson equation. The final velocity and pressure fields are computed using the velocity and pressure correction equations, respectively. The horizontal and vertical domain sizes are 100 and 150 m, respectively, and the grid interval is 1 m in both directions. The time step used is 0.05 s. The initial conditions for wind velocities and turbulent kinetic energy and its dissipation are specified as follows:

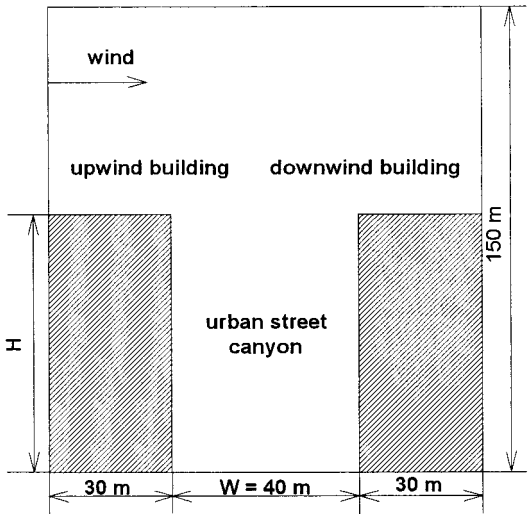

FIG. 2. The model domain configuration for this study.

$$U_0 = 2.5\left(\frac{z}{10}\right)^{0.299}, \quad (10)$$

$$W_0 = 0, \quad (11)$$

$$k_0 = 0.003U_0^2, \quad (12)$$

and

$$\varepsilon_0 = \frac{C_\mu^{3/4}k_0^{3/2}}{\kappa z}. \quad (13)$$

Here, U_0 is in meters per second, z is in meters, and κ is the von Kármán constant (=0.4). Figure 2 shows the model domain configuration for this study. Initially, the shear layer given by (10) is assumed to exist up to z = 10 m above the building roof level and above it velocity is assumed to be constant. Numerical experiments are performed for different values of the street aspect ratio. For this, the building height (H) varies with the width between buildings (W) held fixed (40 m). No-slip boundary conditions are applied to all solid surfaces (Lee and Park 1994). At the inflow boundary, the inflow remains unchanged with time, which has a shear layer up to z = 10 m above the roof level and a shear free layer above it. At the outflow and upper boundaries, the gradient of any variable is set to zero.

3. Results and discussion

a. Flow characteristics

To examine the effects of the street aspect ratio (H/W) on the flow field in urban street canyons, eight numerical experiments are performed with the building heights of

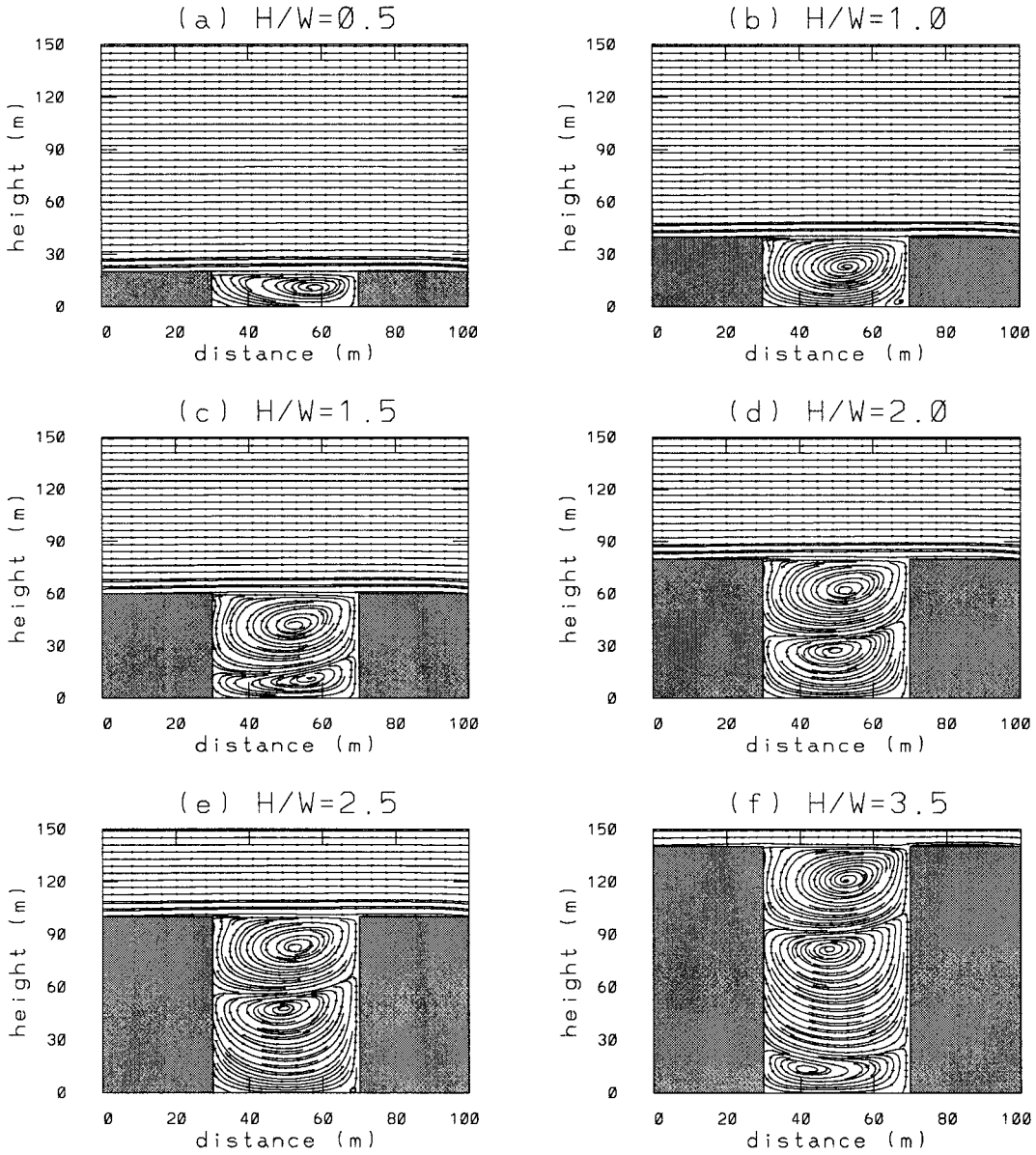

FIG. 3. Streamline fields at $t = 1$ h for street aspect ratios of (a) 0.5, (b) 1, (c) 1.5, (d) 2, (e) 2.5, and (f) 3.5.

16, 20, 40, 60, 80, 100, 120, and 140 m. For the fixed width between buildings (40 m), these building heights correspond to aspect ratios of 0.4, 0.5, 1, 1.5, 2, 2.5, 3, and 3.5, respectively. Results showed that the case with an aspect ratio of 0.4 belongs to the wake interference flow regime. For an aspect ratio of 0.5, it is not clear at first glance whether this case belongs to the wake interference flow regime or the skimming flow regime. However, if we follow the flow identification by Hunter et al. (1990/91), this case appears to be closer to the wake interference flow regime than the skimming flow regime. The other six cases belong to the skimming flow regime. Therefore, a transition from the wake interference flow regime to the skimming flow regime occurs at a threshold aspect ratio between 0.5 and 1. This range of aspect ratio contains the transitional threshold value of 0.67 in the numerical study by Sini et al. (1996).

Figure 3 shows the streamline fields at $t = 1$ h for aspect ratios of 0.5, 1, 1.5, 2, 2.5, and 3.5. After the numerical model experiences an initial adjustment stage, quasi-steady state in the flow field is established after $t = 600\sim1800$ s. This figure clearly shows that the skimming flow regime is characterized by a vortex or vortices almost completely trapped within the street canyon and that the vortex number varies with the aspect ratio. When the aspect ratio is 1, one vortex is formed. When the aspect ratio is 1.5, 2, and 2.5, two counterrotating vortices are formed. When the aspect ratio is

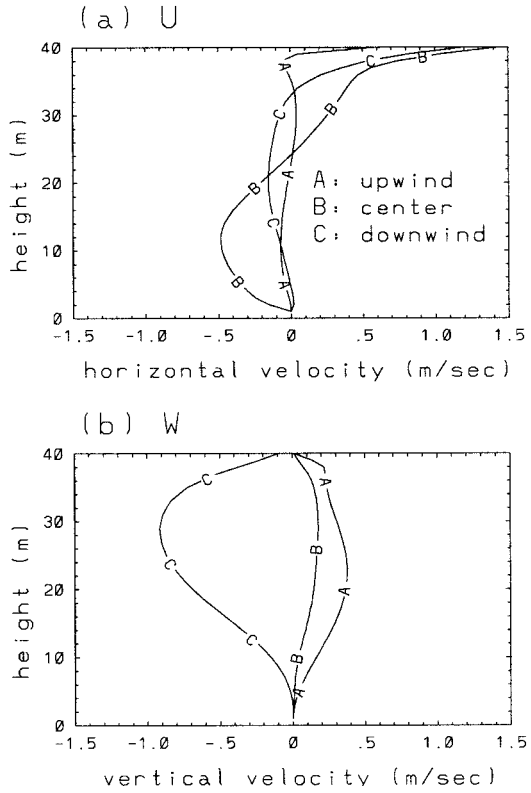

FIG. 4. The vertical profiles of the (a) horizontal and (b) vertical velocities at $x = 33$ m (near the upwind building), $x = 50$ m (at the center of the street canyon), and $x = 67$ m (near the downwind building) at $t = 1$ h for an aspect ratio of 1.

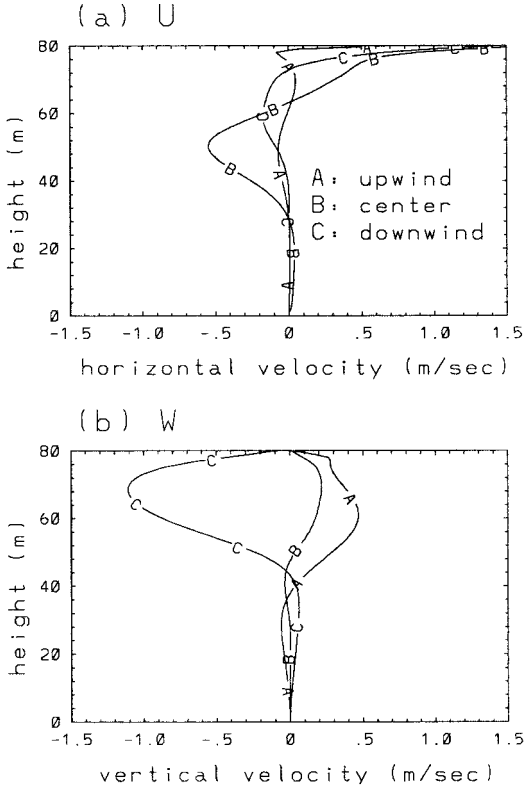

FIG. 5. The same as in Fig. 4 except for an aspect ratio of 2.

3.5, three counterrotating vortices are formed. A threshold aspect ratio between the one-vortex and the two-vortex regimes lies between 1 and 1.5. A threshold aspect ratio between the two-vortex and the three-vortex regimes lies between 3 and 3.5. It is interesting to note that the vortex is asymmetric about its center.

A wind tunnel study by Hoydysh and Dabberdt (1988) showed that for the even notch situation with an aspect ratio of 1.2 the mean ascending vertical velocity is 0.26 ($\pm$0.07) m s^{-1} and the mean descending vertical velocity is 0.24 ($\pm$0.13) m s^{-1} when observations are scaled. To test the present model predictions against the wind tunnel data, a similar numerical experiment with an aspect ratio of 1.2 was performed. It was shown that the mean upward velocity is 0.21 m s^{-1} and the mean downward velocity is 0.26 m s^{-1}. This result is similar to that by Hoydysh and Dabberdt (1988).

The vertical profiles of the horizontal and vertical velocities at $x = 33$ m (near the upwind building), $x = 50$ m (at the center of the street canyon), and $x = 67$ m (near the downwind building) for an aspect ratio of 1 are shown in Fig. 4. These profiles are at $t = 1$ h. The horizontal wind direction at the center of the street canyon changes at $z = 24$ m. This height corresponds to the height of the vortex center, as can be seen in the streamline field (Fig. 3b). The vertical velocity approaches zero at the building roof level ($z = 40$ m). This is an important feature of the skimming flow and results from the spatial limitation between the buildings and the suppression of the upward motion by the ambient wind that plays a role of a lid for the street canyon. The vortex is maintained by the momentum transfer from the ambient wind. The downward motion near the downwind building is stronger than the upward motion near the upwind building. The maximum downward motion is observed at the height of about three-quarters of the building height. These features of the wind profiles are qualitatively in good agreement with the field observation by DePaul and Sheih (1986).

Figure 5 shows the vertical profiles of the horizontal and vertical velocities for an aspect ratio of 2. The vertical profiles of the horizontal and vertical velocities in the upper region above $z \sim 40$ m are similar to those for an aspect ratio of 1 (Fig. 4). However, the magnitudes of the horizontal and vertical velocities in the lower region are small compared with those in the upper layer. This is because the magnitude of the momentum transfer from the upper region into the lower region is smaller than that into the upper layer by the ambient wind. The horizontal wind at the center of the street canyon changes its direction at $z = 29$ and 63 m. These heights correspond to those of the vortex centers in the lower and upper regions of the street canyon, respectively (Fig. 3d). Therefore, it is possible to deduce the

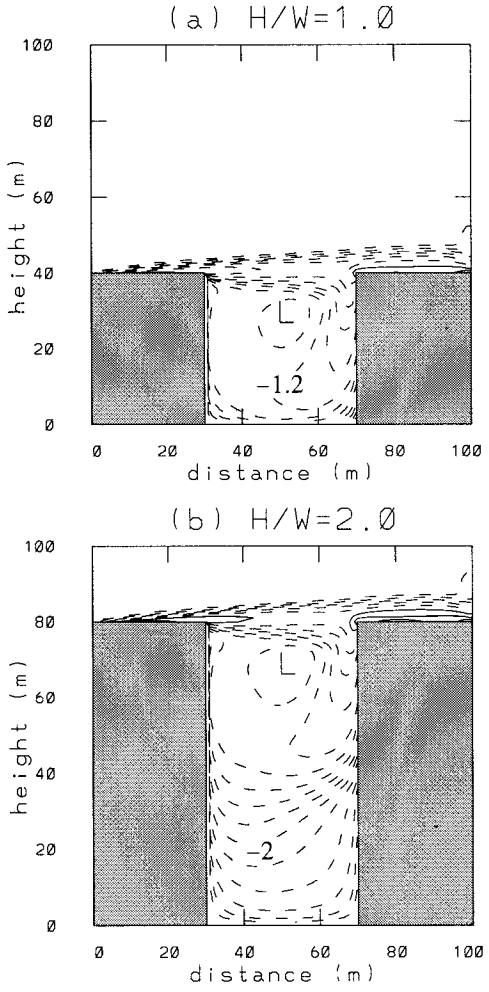

FIG. 6. The fields of turbulent kinetic energy (log scale in base 10) at $t = 1$ h for aspect ratios of (a) 1 and (b) 2. The units are $m^2\ s^{-2}$ and the contour interval is 0.2.

height(s) of the vortex center(s) from the vertical profile of the horizontal velocity at the center of a street canyon.

Turbulent kinetic energy is one of the important quantities representing turbulence intensity. TKE is produced by buoyancy (if the thermodynamic energy equation is included) and wind shear and dissipated by viscosity in the turbulent flow. In order to maintain turbulence, the production of TKE must continue. Figure 6 displays the fields of TKE in a log scale for aspect ratios of 1 and 2. High values of TKE are observed near the rooftop of both buildings because of the strong vertical shear of the horizontal velocity there. This is consistent with the result by Zhang et al. (1996). In the upper-canyon region, TKE is higher near the downwind building than near the upwind building. This is because the vertical shear of the horizontal velocity and the horizontal shear of the vertical velocity on the downwind side of the upper-canyon region are stronger than those on the upwind side.

To understand the relative importance of physical processes associated with TKE in the street canyon, the TKE budget is calculated. Figure 7 shows the vertical profiles of various terms in the TKE equation at $x = 33$ m (near the upwind building), $x = 50$ m (at the center of the street canyon), and $x = 67$ m (near the downwind building) in the case of an aspect ratio of 1. The TKE equation contains the terms of the time tendency, horizontal advection, vertical advection, horizontal diffu-

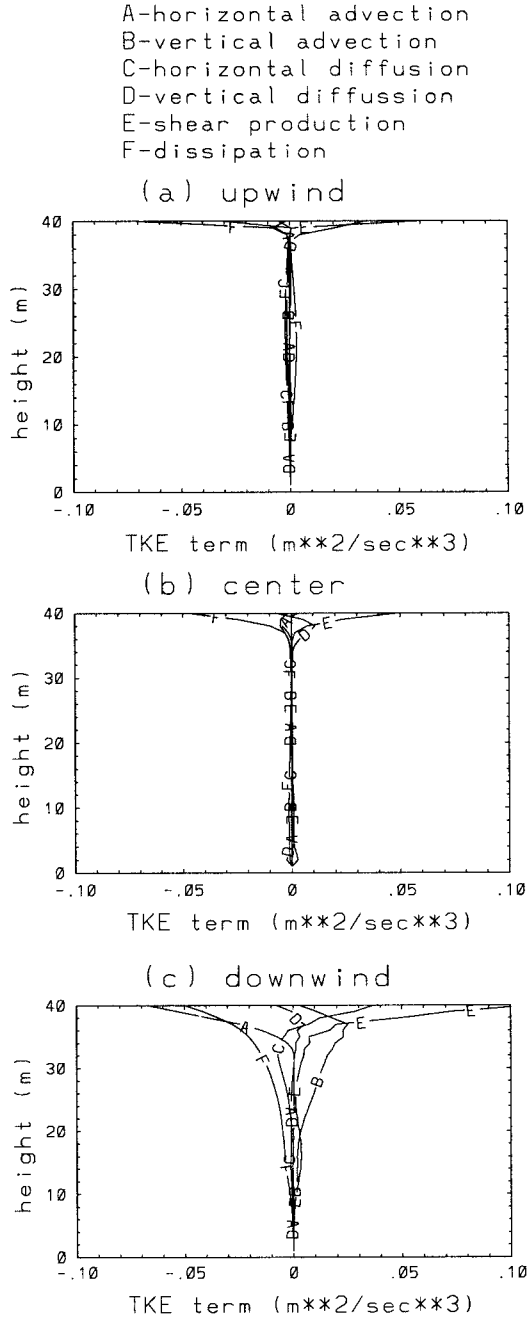

FIG. 7. The vertical profile of each term in the turbulent kinetic energy equation at (a) $x = 33$ m (near the upwind building), (b) $x = 50$ m (at the center of the street canyon), and (c) $x = 67$ m (near the downwind building) at $t = 1$ h for an aspect ratio of 1.

sion, vertical diffusion, shear production, and dissipation. The magnitude of the time tendency term is very small compared with the magnitudes of other terms because the flow field at $t = 1$ h is quasi-steady. At the upwind location (Fig. 7a), the shear production is high near the interface between the ambient flow and the vortex at the roof level, where the turbulent dissipation is also high. Near the roof level, the vertical diffusion contributes to an increase in TKE. At the center location (Fig. 7b), similar to the upwind location, the shear production and turbulent dissipation are high near the roof level. The magnitude of each term in the TKE equation at the downwind location (Fig. 7c) is generally large, especially in the middle and upper regions of the street canyon, compared with that at the upwind or center location. In the upper region of the downwind location, the shear production and turbulent dissipation are high and their magnitudes increase with height. The horizontal advection above $z \sim 32$ m acts to decrease TKE, while the vertical advection acts to increase TKE with its maximum at $z = 37$ m. In the upper region of the downwind location, the horizontal diffusion below (above) $z \sim 36$ m contributes to a decrease (an increase) in TKE.

Figure 7 indicates that the shear production is high near the interface between the ambient flow and the street canyon flow, where the vertical shear of the horizontal velocity is strong. Figure 7 also indicates that the turbulent dissipation is high in the region where the shear production is high. It was shown that the patterns of TKE budget profiles in the upper region for an aspect ratio of 2 are similar to those for an aspect ratio of 1, but the magnitude of each term in the lower region is smaller than that of corresponding term in the upper region.

As shown in Figs. 3–5, the flow field in the urban street canyon is characterized mainly by the number and intensity of vortices produced in the street canyon. Therefore, it seems natural to ask what process is responsible for determining the number of vortices. To answer this question, we consider a case where two vortices are formed in the street canyon. For that case, four numerical experiments are performed in which each horizontal advection term, vertical advection term, horizontal diffusion term, and vertical diffusion term in both the horizontal and vertical momentum equations is excluded for each experiment. Figure 8 shows the streamline fields obtained from these numerical experiments for an aspect ratio of 2. Note that two vortices are formed in the street canyon in the case of an aspect ratio of 2 (Fig. 3d). When the horizontal advection term is excluded in both the horizontal and vertical momentum equations, only one vortex is formed and the center of the vortex is located at $z = 59$ m (Fig. 8a). When the vertical advection term is excluded (Fig. 8b), two vortices are formed. The center of the upper (lower) vortex is located above (below) that in Fig. 3d, and the vertical size of the upper vortex is larger than that of the lower vortex. When the horizontal diffusion term is excluded, only one vortex is formed with its center located at $z = 30$ m (Fig. 8c). When the vertical diffusion term is excluded, five vortices are formed (Fig. 8d). Figure 8 suggests that the horizontal advection and horizontal diffusion terms play a crucial role in the vortex splitting into two or more.

For the two-vortex case, the vortex generation in the lower region of the street canyon is associated with the momentum transfer from the upper region of the street canyon. Also, the momentum is continuously transferred across the roof level from the ambient flow into the street canyon flow. If the ambient wind above the roof level were suddenly set to zero starting from any integration time, the vortex (vortices) in the street canyon would eventually disappear because of the absence of the momentum source.

To investigate the effect of the ambient wind on the vortex generation, numerical experiments are performed in which the initial wind speed at the reference level ($z = 10$ m), denoted by U_{10}, varies from 0.5 to 4 m s^{-1} [see (10)] with a fixed aspect ratio. Figure 9 shows the streamline fields with $U_{10} = 1$, 1.1, 1.3, 1.5, 2, and 4 m s^{-1} for an aspect ratio of 2. Note that U_{10} is 2.5 m s^{-1} in the case of Fig. 3d. The wind profile given by (10) with $U_{10} = 1$, 1.1, 1.3, 1.5, 2, and 4 m s^{-1} gives, for example, ambient wind speeds of 1.87, 2.06, 2.43, 2.80, 3.74, and 7.48 m s^{-1} at $z = 81$ m (1 m above the roof level) (denoted by U_r). In the case of $U_{10} = 0.5$ m s^{-1} ($U_r = 0.93$ m s^{-1}), the ambient wind speed at the roof level is weak and the momentum transfer into the lower region of the street canyon is so small that only one elongated vortex with its center located at an upper level of the street canyon is formed (not shown here). The streamline field in the case of $U_{10} = 1$ m s^{-1} ($U_r = 1.87$ m s^{-1}) (Fig. 9a) is similar to that in the case of $U_{10} = 0.5$ m s^{-1} ($U_r = 0.93$ m s^{-1}) except that small vortices are generated on both sides of the lower region. As the ambient wind speed further increases, the lower vortex increases its intensity and size (Figs. 9b–d). The streamline field in the case of $U_{10} = 2$ m s^{-1} ($U_r = 3.74$ m s^{-1}) (Fig. 9e) is similar to that in the case of $U_{10} = 4$ m s^{-1} ($U_r = 7.48$ m s^{-1}) (Fig. 9f). However, the vortex intensity increases as the ambient wind speed increases. Figure 9 indicates that there is a critical value of the ambient wind speed above which the vortex number and distribution pattern remain the same regardless of the ambient wind speed.

b. Dispersion characteristics

So far, we have examined the flow characteristics in street canyons. Now, we will examine the characteristics of pollutant dispersion in street canyons. The local time tendency of the concentration of a passive pollutant is determined by the horizontal advection, vertical advection, horizontal diffusion, vertical diffusion, and source or sink of pollutants [see (4)]. That is, the pollutant

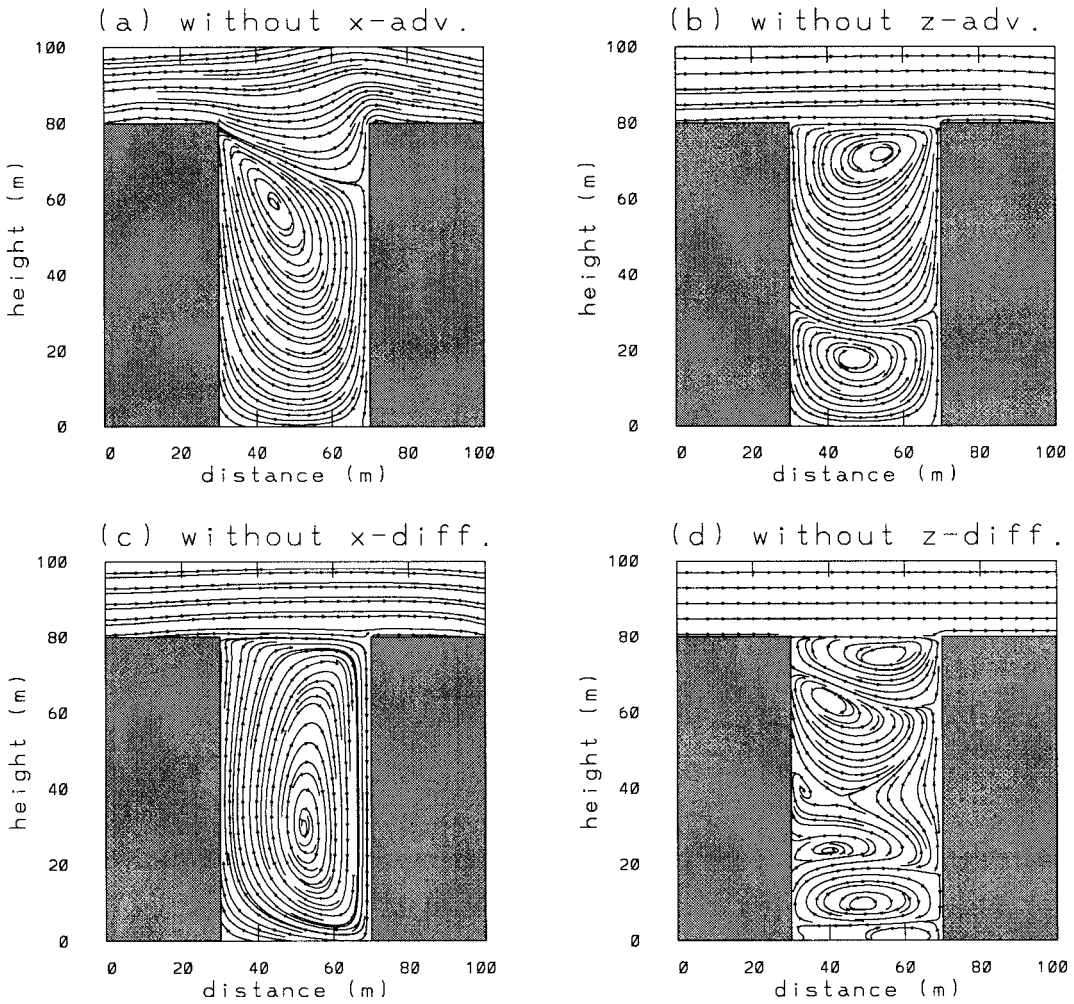

FIG. 8. Streamline fields at $t = 1$ h for an aspect ratio of 2 when we exclude the (a) horizontal advection term, (b) vertical advection term, (c) horizontal diffusion term, and (d) vertical diffusion term in both the horizontal and vertical momentum equations.

distribution is controlled by the grid-scale flow field and the subgrid-scale turbulence, which, in turn, is related to the grid-scale flow field. In this section, we will demonstrate how the flow field affects pollutant dispersion in street canyons.

For this, two cases with different emission sources (street-level source and advected source) are considered. For each case of the emission sources, numerical experiments are performed for urban street canyons with street aspect ratios of 1 and 2, which correspond to the one-vortex and two-vortex flow regimes, respectively (Figs. 3b and 3d). The case of the street-level source, which can be regarded as representing the case of pollutant emission from motor vehicles, is set to have 40 emission points located at street level from the upwind building right edge to the downwind building left edge. The emission rate at each grid point of the street level is 5 ppb s^{-1}. The case of the advected source, which can be regarded as representing the case that pollutants are transported from some other region, is set to have the same total emission amount as the street-level source case. Pollutants are emitted at the inflow boundary from the building roof level to the model top level at the rates of 200/110 ppb s^{-1} and 200/70 ppb s^{-1} in the cases of aspect ratios of 1 and 2, respectively. Note that the number of emission grid points in the advected source case (110 and 70 grid points for aspect ratios of 1 and 2, respectively) is different from that in the street-level source case (40 grid points). In this study, we separately integrate the concentration Eq. (4) for 4 h using the flow fields at $t = 1$ h. We analyze pollutant dispersion when 1) the pollutant emission continues and 2) the pollutant emission suddenly stops. For this, pollutants are continuously emitted at the source points during the first 2 h of the numerical integration and then the emission stops during the next 2 h of the integration.

Figure 10 shows the pollutant concentration fields with a time interval of 1 h in the street-level source

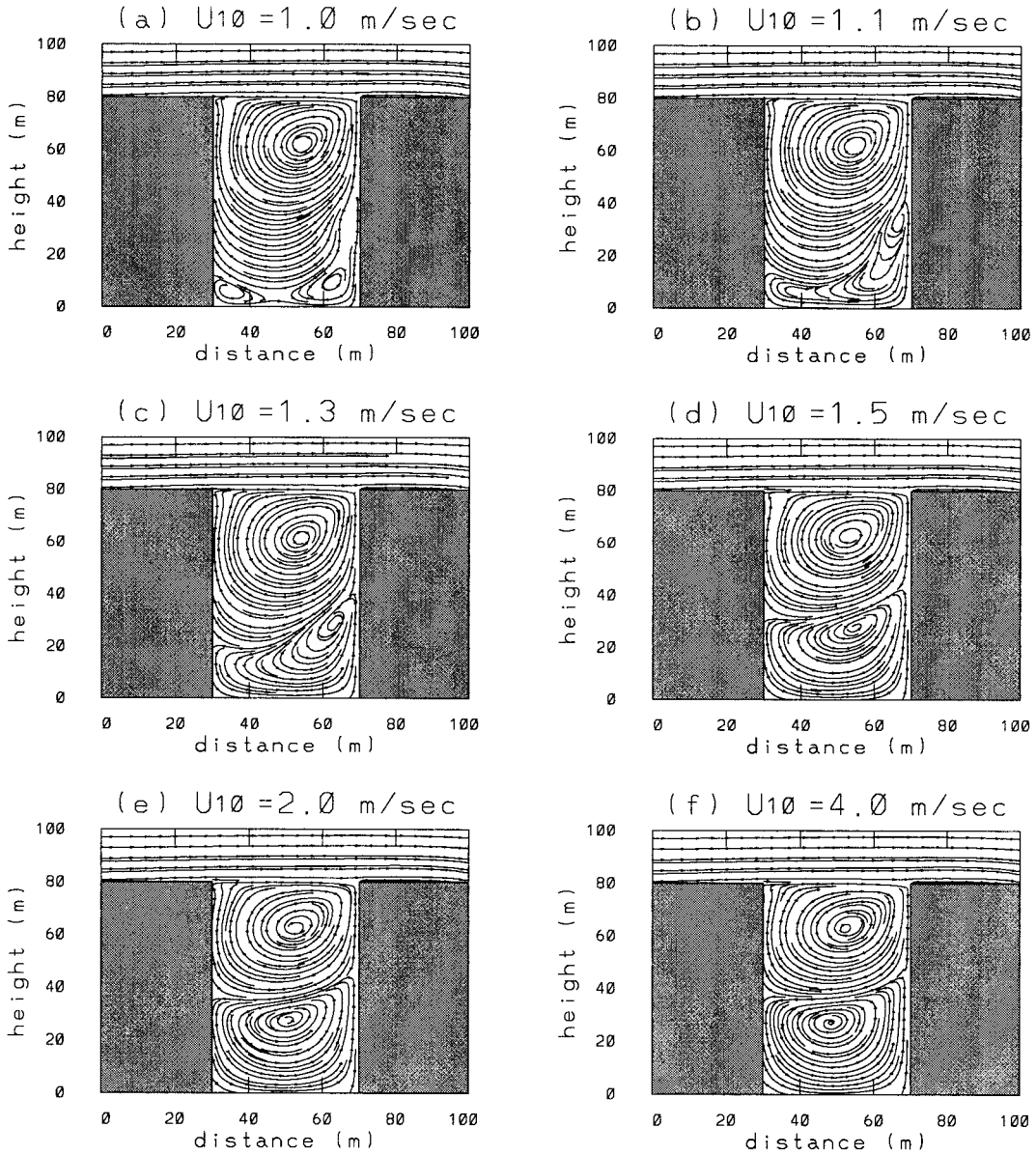

FIG. 9. Streamline fields at $t = 1$ h for an aspect ratio of 2 with different initial wind profiles. The initial wind speeds at the reference height ($z = 10$ m) are (a) 1, (b) 1.1, (c) 1.3, (d) 1.5, (e) 2, and (f) 4 m s^{-1}.

case with an aspect ratio of 1. The concentration is shown on a log scale. During the period of continuous emission (Figs. 10a and 10b), the low-concentration region at any height of the street canyon is located on the downwind side very close to the downwind building, where the strong downward motion exists. This is because the ambient air with relatively very low concentration enters the street canyon by the downward vortex circulation on the downwind side. On the other hand, high concentration at any height of the street canyon is observed on the upwind side close to the upwind building, where the strong upward motion exists, and the concentration on the upwind side decreases upward. This is because highly polluted air passing through the street-level source is advected upward on the upwind side. Once the pollutants reach the roof level, some portion of the pollutants enters the street canyon and other portion escapes from the street canyon. Concentration budget analysis showed that the pollutant escape from the street canyon is dominated by vertical diffusion.

After the emission stops (Figs. 10c and 10d), the concentration contours are closed curves and the maximum concentration is observed at the concentric center of the closed contours that corresponds to the center of the vortex. The pollutant concentration at any point of the street canyon exponentially decreases with time after the emission stops. This is somewhat an expected result

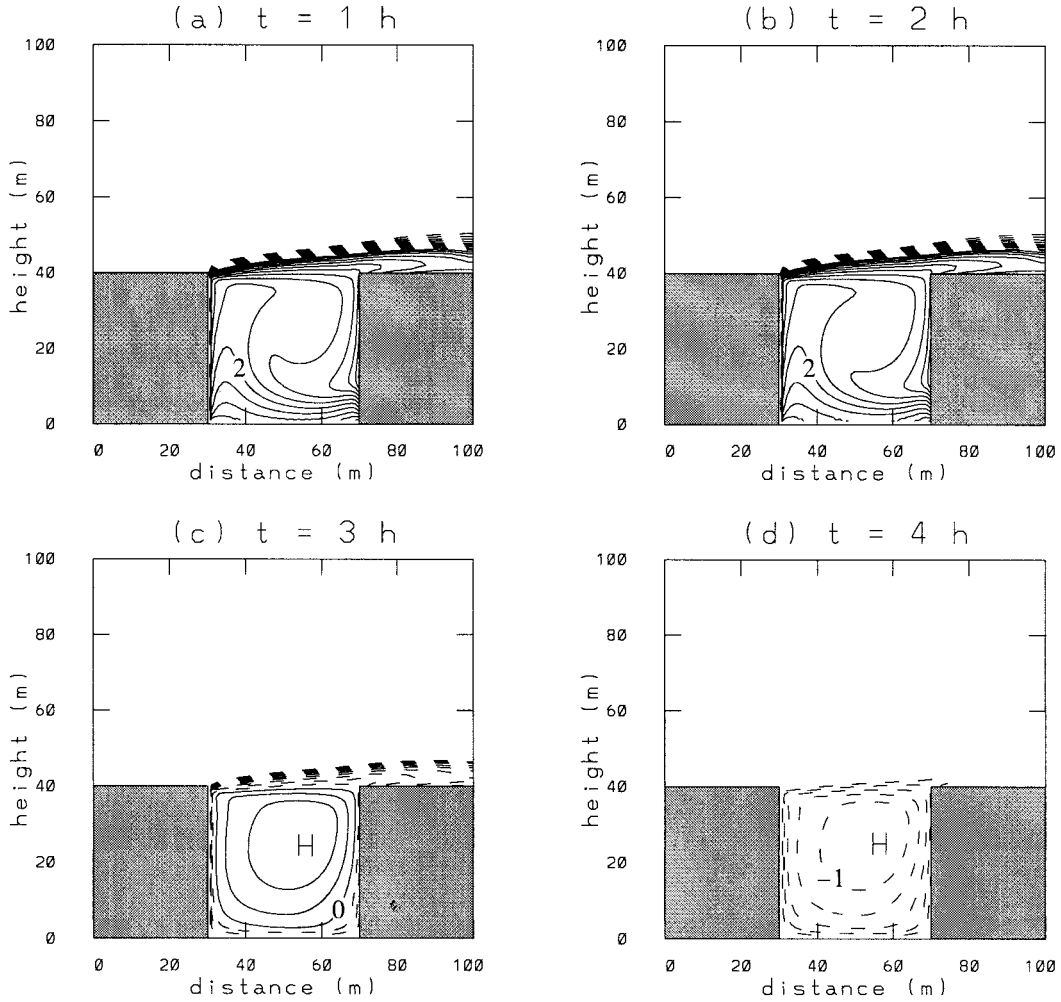

FIG. 10. The fields of pollutant concentration (log scale in base 10) at t = (a) 1 h, (b) 2 h, (c) 3 h, and (d) 4 h for an aspect ratio of 1 in the case of the street-level source. The units are ppb and the contour interval is 0.2.

from the diffusion equation and is also true for the cases presented in Figs. 11, 12, and 13. Lee and Park (1994) suggested that in the street canyon pollutant transport along streamlines is mainly due to advection by the mean wind, while pollutant transport across streamlines is mainly due to diffusion. Therefore, pollutants in outer streamlines can rapidly escape from the street canyon after being transported to the roof level, while pollutants near the vortex center require more time to escape from the street canyon.

Figure 11 is the same as in Fig. 10 except for an aspect ratio of 2. During the first 2 h of continuous emission from the street-level source (Figs. 11a and 11b), the pattern of the concentration distribution in the upper region of the street canyon ($\sim$40 m $\leq z \leq$ 80 m) is similar to that in the case of the street-level source with an aspect ratio of 1 (Figs. 10a and 10b). However, the pattern of the concentration distribution in the lower region is different from that in the upper region. In spite of its difference in the upper and lower regions, observed is a common feature that high (low) concentration at any height of the upper or lower region appears in the region of the upward (downward) motion, that is, on the downwind (upwind) side of the lower region and the upwind (downwind) side of the upper region. This feature is directly linked to the two-vortex circulation (Fig. 3d). Highly polluted air passing through the street-level source is advected upward on the downwind side of the lower region with the concentration decreasing with height. Near the midlevel, pollutants are transported from the downwind side to the upwind side. On the upwind side, pollutants are transported either upward by the upward motion of the upper vortex or downward by the downward motion of the lower vortex. The ambient air with relatively very low concentration enters the street canyon by the downward motion of the upper vortex on the downwind side. This explains the common feature in the pattern of the concentration distribution mentioned above.

After the emission from the street-level source stops

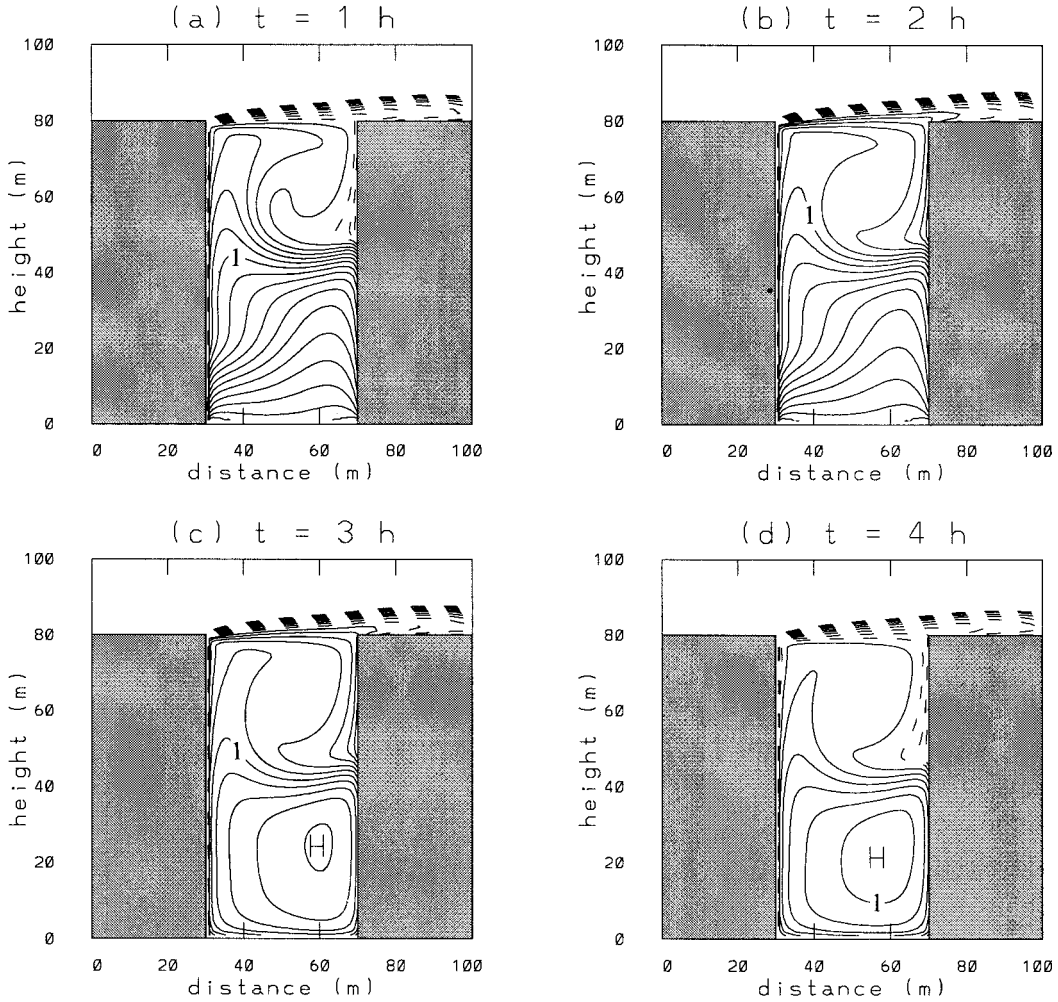

FIG. 11. The same as in Fig. 10 except for an aspect ratio of 2.

(Figs. 11c and 11d), the pattern of the concentration distribution in the lower region is similar to that in the one-vortex case (Figs. 10c and 10d). Although the emission stops, in the upper region there still exists a similar distribution pattern to that in the one-vortex case with continuous emission (Figs. 10a and 10b). This is because pollutants transported from the lower region by both the advection and diffusion act as a secondary emission source near $z = 40$ m for the upper region. Figures 10 and 11 indicate that in the street-level source case the distribution of pollutant concentration in the street canyon can be largely explained in terms of the vortex circulation.

The pollutant concentration fields in the case of the advected source with an aspect ratio of 1 is shown in Fig. 12. During the period of continuous pollutant advection (Figs. 12a and 12b), the plume of pollutants is advected above the street canyon and some fraction of it is transported from the roof level into the street canyon. The downward vertical advection of the highly polluted ambient air on the downwind side of the street canyon results in higher concentration on the downwind side than on the upwind side. This result is qualitatively similar to that of the numerical experiment (Sini et al. 1996) in which a pollutant cloud is passing above the street canyon during a short time period. After the pollutant advection stops (Figs. 12c and 12d), pollutants trapped in the street canyon start to drain into the ambient air through the same process mentioned in the street-level source case (Figs. 10c and 10d).

Figure 13 shows the pollutant concentration fields in the advected source case with an aspect ratio of 2. During the period of continuous pollutant advection (Figs. 13a and 13b), a main pathway of pollutant inflow into the street canyon is on the downwind side of the upper region of the street canyon, where the maximum concentration appears through the vertical advection by the strong downward motion. At any level of the lower region of the street canyon, high concentration is observed on the upwind side because of the downward advection of relatively polluted air there. Once the pollutant advection stops (Figs. 13c and 13d), the pattern

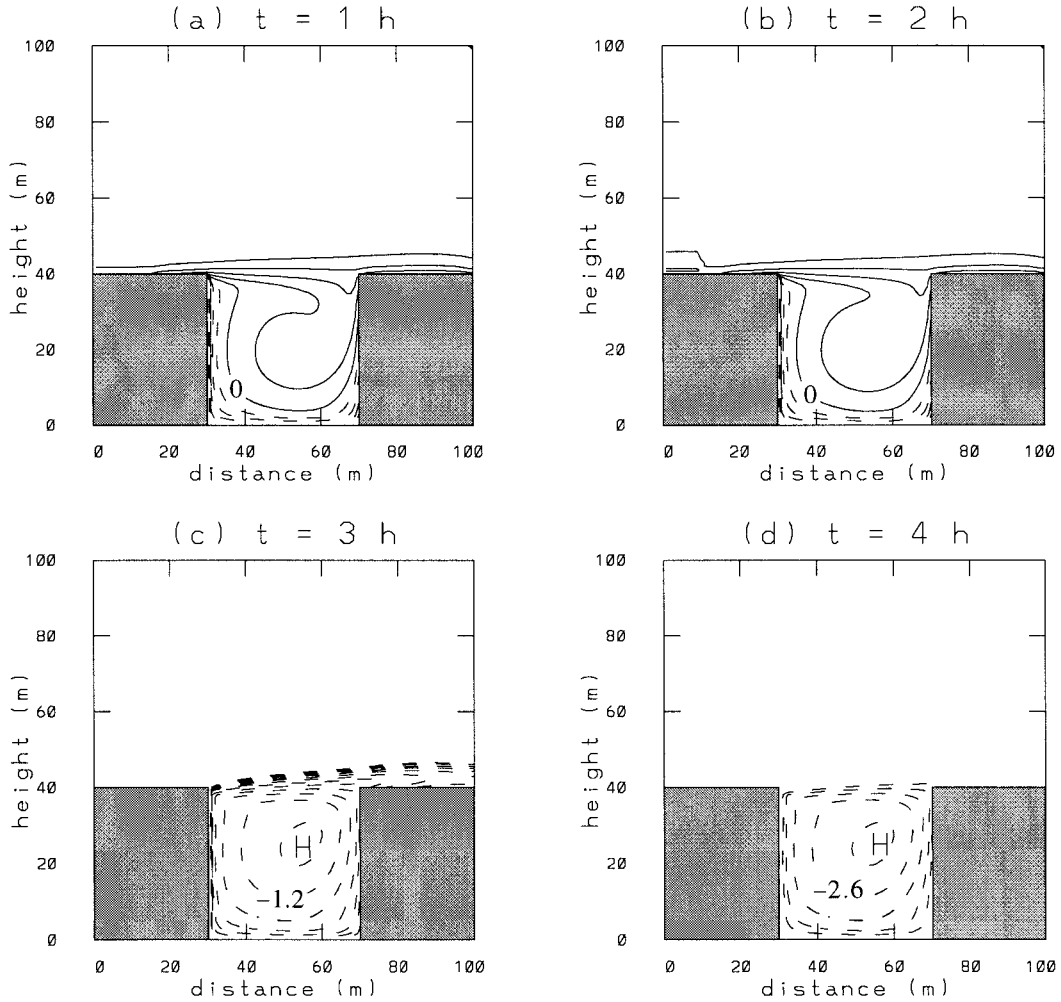

FIG. 12. The fields of pollutant concentration (log scale in base 10) at t = (a) 1 h, (b) 2 h, (c) 3 h, and (d) 4 h for an aspect ratio of 1 in the case of the advected source. The units are ppb and the contour interval is 0.2.

of the concentration field is similar to that in the street-level source case (Figs. 11c and 11d). A secondary emission source is formed near the midlevel of the street canyon and gives the same effect on the concentration distribution in the upper region as the street-level source case with an aspect ratio of 2 does (Figs. 11c and 11d). As in the street-level source case (Figs. 10 and 11), in the advected source case (Figs. 12 and 13) the distribution of pollutant concentration in the street canyon can be largely explained in terms of the vortex circulation.

4. Summary and conclusions

In this study, the flow and pollutant dispersion in urban street canyons were investigated using a two-dimensional numerical model with the k–ε turbulent closure scheme. It was shown that the number and intensity of vortices mainly characterize the flow field in the street canyon and that the number of vortices increases with increasing street aspect ratio (ratio of the building height to the width between buildings). The vertical velocity approaches zero at the roof level of the street canyon. In the upper-canyon region, the downward motion near the downwind building is stronger than the upward motion near the upwind building. Also, the turbulent kinetic energy (TKE) is higher near the downwind building than near the upwind building because of stronger wind shears near the downwind building. The TKE budget analysis showed that the shear production is high near the interface between the ambient flow and the street canyon flow and that the turbulent dissipation is also high in the region of high shear production. It was found that horizontal advection and diffusion play a crucial role in splitting the vortex into two or more. It was also found that there is a critical value of the ambient wind speed above which the number and distribution pattern of vortices remain the same regardless of the ambient wind speed.

To examine pollutant dispersion in urban street can-

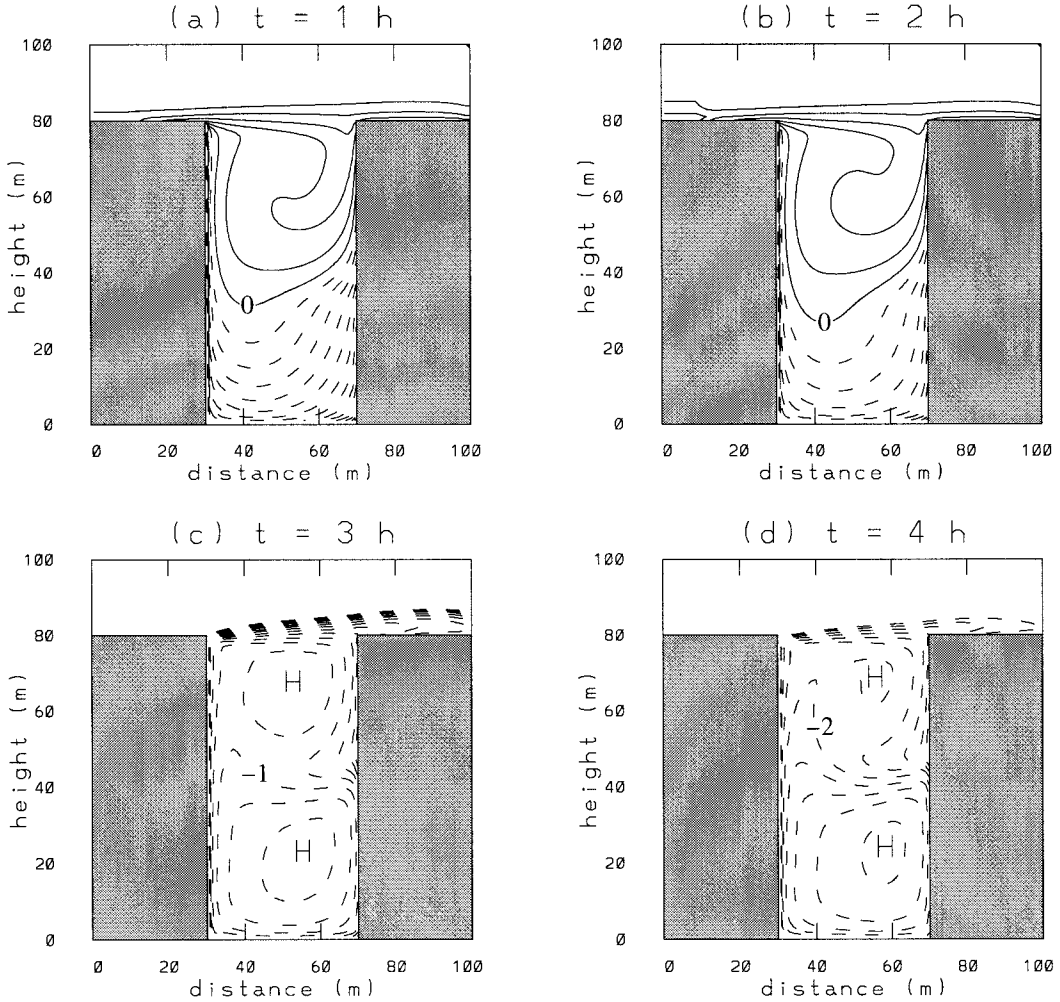

FIG. 13. The same as in Fig. 12 except for an aspect ratio of 2.

yons with different pollutant emission sources and aspect ratios, the cases of the street-level source and the advected source with aspect ratios of 1 (one-vortex regime) and 2 (two-vortex regime) were considered for the given flow fields. Results indicated that the distribution of pollutant concentration in the street canyons during each period of continuous emission and nonemission can be largely explained in terms of the vortex circulation.

In this study, thermal effects on the flow and pollutant dispersion were not considered. During the daytime, the building walls and street are heated depending on the solar zenith angle and meteorological conditions. When the building wall (or street) is heated, the air parcel adjacent to it acquires buoyancy, and the flow field in the street canyon can be affected by the heating (Sini et al. 1996). A study of including the thermodynamic energy equation in the present model and systematically examining thermal effects on the flow and pollutant dispersion in urban street canyons is needed. In this study, two-dimensional geometry was considered; that is, infinitely long buildings and street canyon were assumed. A study of including the third dimension in the current model and examining three-dimensional flow and pollutant dispersion in urban street canyons would enable us to understand interesting phenomena that cannot be obtained from the two-dimensional simulations. These two research areas are under investigation.

Acknowledgments. The authors are very grateful to Dr. In Young Lee at the Argonne National Laboratory for providing his original model code. This research was supported by Cray Research, Inc., through the 1998 University Research and Development Grant of the Systems Engineering Research Institute (SERI), Korea, and the Korea Ministry of Science and Technology.

REFERENCES

DePaul, F. T., and C. M. Sheih, 1986: Measurements of wind velocities in a street canyon. *Atmos. Environ.,* **20,** 455–459.

Hoydysh, W. G., and W. F. Dabberdt, 1988: Kinematics and dispersion

characteristics of flows in asymmetric street canyons. *Atmos. Environ.,* **22,** 2677–2689.

Hunter, L. J., I. D. Watson, and G. T. Johnson, 1990/91: Modelling air flow regimes in urban canyons. *Energy Bldg.,* **15–16,** 315–324.

——, G. T. Johnson, and I. D. Watson, 1992: An investigation of three-dimensional characteristics of flow regimes within the urban canyon. *Atmos. Environ.,* **26B,** 425–432.

Hussain, M., and B. E. Lee, 1980: An investigation of wind forces on three-dimensional roughness elements in a simulated atmospheric boundary layer flow. Part II: Flow over large arrays of identical roughness elements and the effect of frontal and side aspect ratio variations. University of Sheffield Department of Building Science Rep. BS-56, 81 pp.

Hussein, H. J., and R. J. Martinuzzi, 1996: Energy balance for turbulent flow around a surface mounted cube placed in a channel. *Phys. Fluids,* **8,** 764–780.

Lanzani, G., and M. Tamponi, 1995: A microscale Lagrangian particle model for the dispersion of primary pollutants in a street canyon. Sensitivity analysis and first validation trials. *Atmos. Environ.,* **22,** 2677–2689.

Lee, I. Y., and H. M. Park, 1994: Parameterization of the pollutant transport and dispersion in urban street canyons. *Atmos. Environ,* **28,** 2343–2349.

Nigim, H. H., 1996: Recovery of equilibrium turbulent boundary layers downstream of obstacles. *Phys. Fluids,* **8,** 548–554.

Oke, T. R., 1988: Street design and urban canopy layer climate. *Energy Bldg.,* **11,** 103–113.

Patankar, S. V., 1980: *Numerical Heat Transfer and Fluid Flow.* McGraw-Hill, 197 pp.

Sini, J.-F., S. Anquetin, and P. G. Mestayer, 1996: Pollutant dispersion and thermal effects in urban street canyons. *Atmos. Environ.,* **30,** 2659–2677.

Zhang, Y. Q., S. P. Arya, and W. H. Snyder, 1996: A comparison of numerical and physical modeling of stable atmospheric flow and dispersion around a cubical building. *Atmos. Environ.,* **30,** 1327–1345.